Journal of Photonics for Energy

PhotonicsforEnergy.SPIEDigitalLibrary.org

Photon management in solution-processed organic light-emitting diodes: a review of light outcoupling micro- and nanostructures

Guillaume Gomard
Jan B. Preinfalk
Amos Egel
Uli Lemmer

SPIE.

Guillaume Gomard, Jan B. Preinfalk, Amos Egel, Uli Lemmer, "Photon management in solution-processed organic light-emitting diodes: a review of light outcoupling micro- and nanostructures," *J. Photon. Energy* **6**(3), 030901 (2016), doi: 10.1117/1.JPE.6.030901.

REVIEW

Photon management in solution-processed organic light-emitting diodes: a review of light outcoupling micro- and nanostructures

Guillaume Gomard,[a,b,*] Jan B. Preinfalk,[a] Amos Egel,[a,b] and Uli Lemmer[a,b]

[a]Karlsruhe Institute of Technology (KIT), Light Technology Institute, Engesserstrasse 13, 76131 Karlsruhe, Germany

[b]Karlsruhe Institute of Technology (KIT), Institute of Microstructure Technology, Hermann-von-Helmholtz-Platz 1, 76344 Eggenstein-Leopoldshafen, Germany

Abstract. To allow a greater acceptance in the display and lighting markets, organic light-emitting diode (OLED) technology is currently the subject of intensive research efforts aimed at manufacturing cost-effective devices with higher efficiencies. In this regard, strategies matured in the field of photonics and nanophotonics can be applied for photon management purposes to improve the outcoupling of the generated light and to control the emission pattern. In this review, we report on the recent experimental and numerical advances to pursue those goals by highlighting the example of bottom-emitting devices. The cases of periodical micro- and nanostructures, as well as of stochastic ensembles that can be easily implemented using printing techniques, are covered herein. It is shown that beyond the sole optical properties, such additional elements can simultaneously improve the electrical characteristics of solution-processed OLEDs, and thus enable an optimization of the devices at different levels. © *The Authors. Published by SPIE under a Creative Commons Attribution 3.0 Unported License. Distribution or reproduction of this work in whole or in part requires full attribution of the original publication, including its DOI.* [DOI: 10.1117/1.JPE.6.030901]

Keywords: organic light-emitting diodes; light outcoupling; microlens array; diffraction gratings; electromagnetic scattering; optical simulations.

Paper 16066MV received May 31, 2016; accepted for publication Jul. 21, 2016; published online Aug. 19, 2016.

1 Theoretical Background and Motivation

The basic principle behind organic light-emitting diodes (OLEDs) is the radiative decay of molecular excited states following the injection and the recombination of charge carriers inside an emitting layer. To achieve this, those devices usually consist of a thin film of organic emissive material (based on conjugated polymers or small molecules) introduced between two electrodes, with at least one being semitransparent. The whole device is typically deposited onto a glass substrate as shown in Fig. 1(a). Additional hole and electron transport layers (HTL and ETL, respectively) may be incorporated within the stack to efficiently transport the injected charge carriers to the emitting layer and avoid charge accumulations, while hole and electron blocking layers can be used to prevent non-radiative recombination at the counter electrode (in the stack depicted, BPhen is used for both purposes but will be referred to as the ETL layer for the sake of simplicity).

One important quantity to assess the performance of OLEDs is the external quantum efficiency (η_{ext}). It is defined as the ratio of the total number of photons emitted out of the device to the number of electrons injected into the emitter, and can be expressed as follows:

$$\eta_{ext} = \eta_{int}\eta_{outcoupling}, \tag{1}$$

where η_{int} is the internal quantum efficiency (ratio of the total number of photons generated inside the emitter to the number of injected electrons) and $\eta_{outcoupling}$ is the external coupling

*Address all correspondence to: Guillaume Gomard, E-mail: guillaume.gomard@kit.edu

This review manuscript is also part of the section on "Breakthroughs in Photonics and Energy," highlighting primarily recent advances in the last three years.

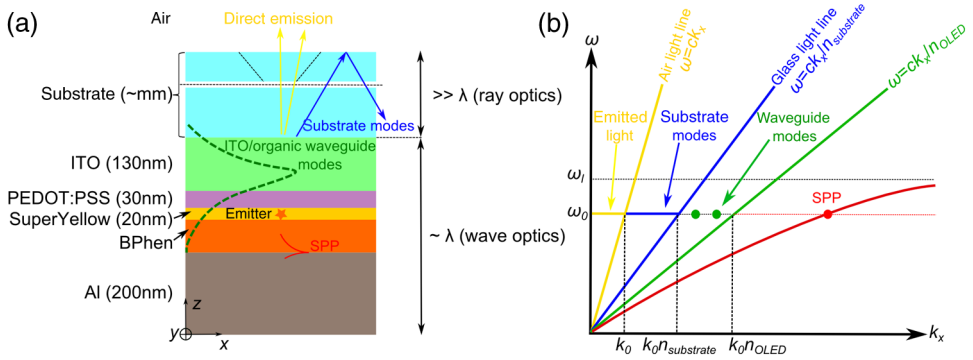

Fig. 1 (a) Bottom-emission planar OLED adapted from Ref. 4 depicted with its optical loss channels and (b) dispersion relation of an OLED represented at a given frequency ω_0. The mode continuum associated with the light emitted out of the device lies above the air light line, while the substrate mode continuum is located between the air and the glass light lines. The discrete waveguide modes propagating within the ITO and organic layers are distributed below the glass light line. Finally, a single SPP mode is depicted in the figure (where ω_l is related to the plasma frequency of the metal considered, among others).

efficiency (ratio of the total number of photons coupled out of the device to the total number of generated photons). Whereas η_{int} can approach 100% by using phosphorescent emitters,[1] in which case nonradiative processes can be neglected, $\eta_{\text{outcoupling}}$ usually stands well below 100% and, therefore, strongly limits the performances of OLEDs.

This can be attributed to the different optical loss channels in the device responsible for the reduced fraction of generated light emitted into air, which can typically reach values of only 20% without suitable photon management approaches. In order to address this point, different concepts have to be invoked for the two main regions in the OLED. The first one is the substrate. In this homogeneous and optically thick medium (the substrate thickness is in the mm range), the light can be considered as incoherent and the optical effects described on the basis of geometrical or ray optics due to the dimensions involved. The corresponding loss channel results from the refractive index mismatch between the substrate ($n_{\text{substrate}} \approx 1.55$ for glass) and the external medium (air, $n_{\text{air}} = 1$) leading to a limited light escape cone. The light impinging on the substrate/air planar interface with an angle larger than the critical angle is subject to total internal reflection (TIR). It is then guided in the so-called substrate modes, damped due to the limited reflectivity of the underlying stack, and can escape through the edges of the device. The second region is formed by the other layers whose thicknesses are comparable or below the wavelength of the emitted photons. As such, wave optics is needed to describe the different coupling schemes taking place in those thin layers. One major optical loss channel is related to waveguide modes propagating within the organic layers and transparent electrodes whose total thickness is of few hundreds of nanometers only. This occurs because the refractive index of those layers (typically ranging from 1.7 to 2.1[2]) is significantly higher than those of the substrate and of the cathode for a large spectral range. Consequently, the OLED stack forms a slab waveguide. The confined light can be parasitically absorbed in the different thin layers or can leak through the edges of the OLED. In addition, emitters located at the vicinity of the metallic cathode (few tens of nanometers from it) can either dissipate their power through ohmic losses by dipolar near-field coupling or via the coupling to surface plasmon polaritons (SPPs).[3] The above-mentioned optical channels are shown in Fig. 1(a) and illustrated in the dispersion diagram $\omega(k_x)$ of Fig. 1(b).

The rigorous computation of the fraction of light confined in the OLED stack under the form of substrate, waveguide, or SPP modes is not straightforward since microcavity effects have to be taken into account. This impacts not only the power injected into the different loss channels but also the spontaneous exciton decay rate which directly depends on its optical environment via the Purcell effect.[3,5,6] In addition, a proper analysis of the device requires the determination of the emitters' orientation together with their distribution profile within the active layer.[7–10]

As an illustration of the previous discussion, we simulated the yellow planar OLED reported in Fig. 1(a) [using the poly(para-phenylene vinylene) (PPV)-based polymer PDY-132 ("Super Yellow"), from Merck KGaA] at the peak emission wavelength (550 nm) and checked the results

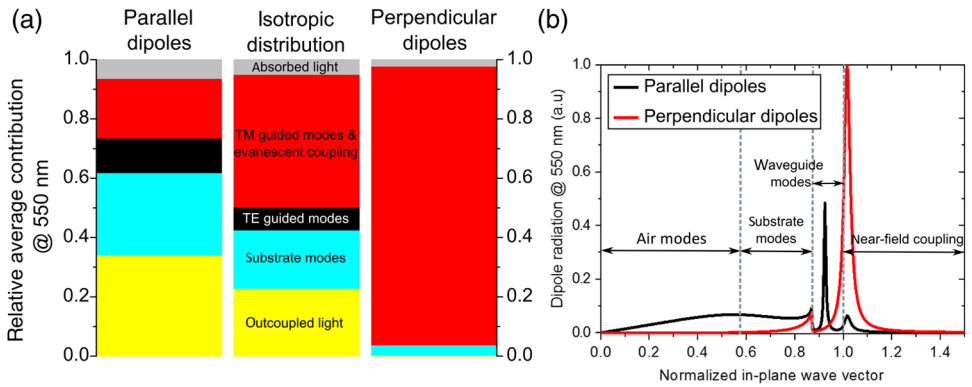

Fig. 2 (a) Contribution of the different optical channels in the planar OLED of Fig. 1 for a parallel or perpendicular dipole moment orientation and for an isotropic distribution (with a contribution of the parallel and of the perpendicular orientations of 2/3 and 1/3, respectively), and (b) dissipated power as a function of the normalized in-plane wave vector $k_{||}/k_{\text{emitter}}$ represented for a parallel and for a perpendicular dipole moment orientation. The ETL layer thickness is set to 60 nm.

with the software "Setfos" from "Fluxim AG."[11] An internal quantum efficiency of 100% was assumed, and the emitting layer was considered as nonabsorbing. In this example, the dipoles were located at the center of the thin emitting layer. In the case of a parallel dipole moment orientation [i.e., in the (xy) plane], which is relevant for thin films made of conjugated polymers,[7,12] Fig. 2(a) shows that only around 34% of the generated light is emitted into air. Indeed, a significant part of the dissipated power is lost due to the coupling to substrate modes (28%), and to a lesser extent to waveguide and evanescent coupled (SPP) modes. The analysis of Fig. 2(b) enables the identification of one waveguide mode and a SPP mode for a normalized in-plane wave vector above 1. In order to test the influence of the dipole moment orientation, an additional power dissipation spectrum was added to Fig. 2(b). It corresponds to a perpendicular orientation of the radiative dipole. A noticeable difference is the sharp increase of the dissipated power related to the coupling with the SPP mode which prevents the light from escaping the OLED stack. Indeed, unlike horizontal dipoles, vertical ones can strongly couple to SPP modes, favoring this loss channel which is then predominant.[9] It should be noted that in the present example, the dipoles-to-cathode distance is 70 nm, which makes the coupling to evanescent modes particularly detrimental.

From Fig. 2, it can be inferred that specific photonic strategies have to be implemented to overcome the optical losses encountered in OLEDs. Moreover, a good knowledge of the system considered is necessary to identify the main loss channels and design adapted outcoupling solutions. A straightforward way to address those issues consists in optimizing the thickness of the different layers involved. For example, the losses induced by the coupling to SPP modes can be minimized by increasing the spacing between the emitters and the cathode, for instance by using a thicker ETL which acts as an optical spacer. In fact, Fig. 3 shows that increasing the ETL thickness leads to an enhanced outcoupling efficiency—but at the same time, the excitation

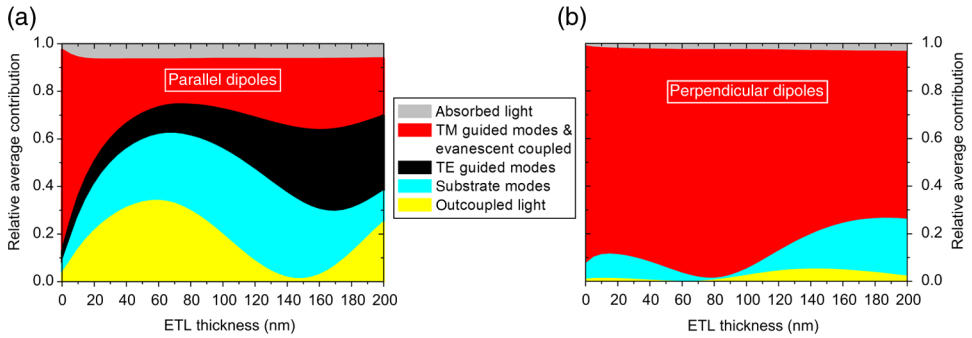

Fig. 3 Contribution of the different optical channels in the planar OLED (at 550 nm) as a function of the ETL thickness for a parallel (a) and a perpendicular (b) dipole moment orientation. In the former case, the fraction of outcoupled light is maximized for an ETL thickness of 60 nm.

of substrate guided modes increases, too. This underlines the need for simultaneously tackling the losses occurring within the thin films stack (to ameliorate the so-called "internal outcoupling"), and in the substrate (improvement of the "external outcoupling").

Beyond those simple design rules, which have the advantage of leaving the global design of the OLED unchanged, more advanced concepts can be exploited by using periodically arranged or disordered micro- and nanostructures at the different levels of the devices. This ongoing topic has already created a rich pool of numerical and experimental studies covered in several reviews.[13–19]

In the present paper, we introduce more specifically the main advances obtained within our research group over the last years, by first focusing on the extraction of substrate modes, and then on the outcoupling of internal modes. This latter aspect will be discussed by separating the cases of micro- or nano-based structures, and of periodic or stochastic configurations. The objective is to highlight relevant and upscalable strategies which can increase the fraction of outcoupled light while maintaining satisfying light output pattern and electrical characteristics of the bottom-emitting OLEDs considered. Focus will be given to solution-processed devices. Although their performance usually stands below that of their vacuum-deposited counterparts, which necessitates approaches to fabricate solution-processed multilayers,[20] they nonetheless open the way for cheap and large-area compatible fabrication processes that can utilize the printing industry facilities.[21]

2 Improvement of the External Outcoupling Through the Introduction of Microlens Arrays

As discussed in Sec. 1, substrate modes retain a significant part of the generated light, with around 28% of the dissipated power in the example of Fig. 2(a) (parallel dipoles). Among the methods employed to cope with this issue, one can mention, e.g., a simple and cost-effective solution based on the roughening of the substrate surface by sandblasting, or the deposition of a scattering layer on top of the substrate, for instance using nanoparticles/polymer host systems or flexible layers made of porous polymers.[14,22] The main drawback of those techniques is that a fraction of the light impinging on the modified surface is redirected toward the thin film stack and experiences losses through the channels already described. In the framework of the studies which advocate the use of cheap and easily up-scalable cellulose-based scattering layers, this issue was recently circumvented by controlling the amount of volume scattering. This is realized by a proper infiltration of the microcavities, e.g., with nanocellulose fibers,[23] or with a plastic layer which additionally improves the layers' durability.[24] An alternative approach for extracting substrate modes consists of introducing a microlens array (abbreviated "MLA" in the following), usually based on hemispheres, which enables to outcouple most of the light after the first interaction and to ensure a Lambertian emission, as is usually desired for applications. This method inspired by the work of Madigan et al.,[25] and further developed by different research groups in the early 2000s,[26–28] is nevertheless hindered by the complexity of its implementation. For this reason, a versatile, reproducible, and upscalable fabrication process was proposed by Bocksrocker et al.[2] and is presented below.

As shown in Fig. 4, the fabrication sequence can be summarized by two main steps, that is, the creation of a Polydimethylsiloxane (PDMS) stamp incorporating the desired features of the MLA (diameter, aspect ratio, and periodicity), and the transfer of this pattern into a polymethylmethacrylate (PMMA) layer deposited on the substrate. It should be noted that due to the chemical and mechanical stability of the PDMS stamp, the latter can be cleaned and reused afterwards.

Microlenses with diameters of 10, 20, and 30 μm (almost equal to the periodicity of the array) and with an aspect ratio of 1 (hemispheres) were fabricated according to this process. The resulting MLAs have a typical transmission above 80% between 400 and 800 nm. Furthermore, their haze factor in transmission, defined as the ratio of the nonspecularly transmitted light to the overall transmitted light, reaches more than 70% regardless of the diameter considered. Thus, MLAs can help diffusing angular and, to a certain extent, spatial inhomogeneities of the emission. However, in case of a large variation in the local brightness, as the one introduced by shadowing metal grids used for charge carrier transport, more advanced concepts are required to obtain a spatially homogeneous emission.[30] In order to test their potential for external outcoupling, those MLAs were integrated in white OLEDs (WOLEDs) by using a single

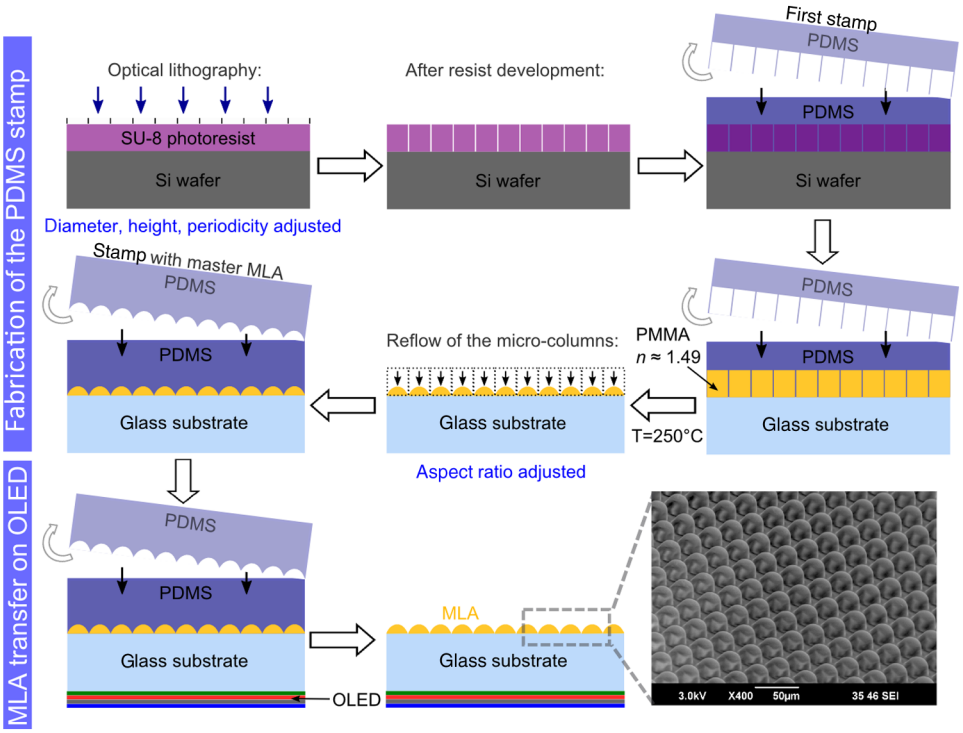

Fig. 4 Overview of the MLA fabrication process (adapted from Ref. 29).

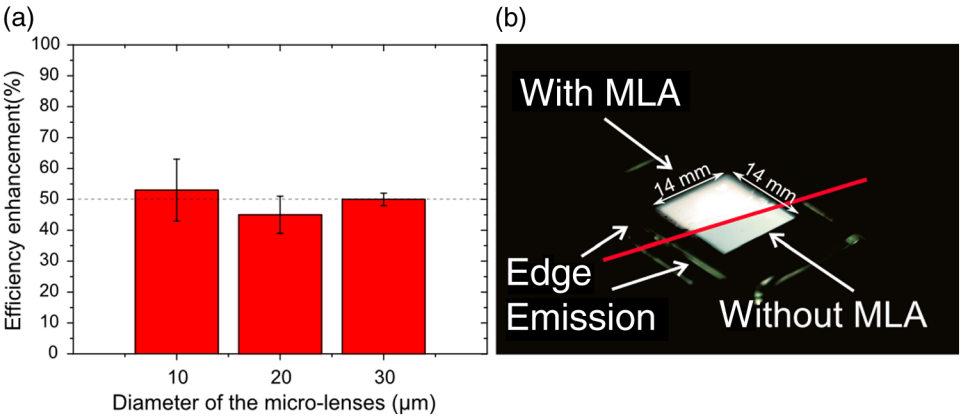

Fig. 5 (a) Efficiency enhancement measured in WOLEDs following the integration of MLAs with different diameters and (b) picture of a WOLED partly covered by a 30-μm diameter based MLA. A weaker edge emission can be noticed for the region covered by the MLA (adapted from Ref. 29).

layer of the white-emitting co-polymer SPW087 by Merck KGaA, and the measured efficiencies (defined in terms of luminous flux normalized to the electrical power consumption) were compared with the ones obtained without the MLA on the same devices.[29] The results shown in Fig. 5 demonstrate that an efficiency enhancement of around 50% is achieved compared to a reference device which exhibits a luminous efficacy of 5 $\mathrm{lm.W^{-1}}$. In addition, the diameter of the micro-lenses has only a weak influence on the enhancement factor, an observation which is corroborated by other studies.[26] It can be added here that most of the light outcoupling was found to occur after the first interaction with the MLA. Lastly, the MLA did not affect the spectral and angular emission characteristics of the WOLEDs investigated. To summarize, the fabrication process presented above enables production of high-quality MLAs on large areas to efficiently extract substrate modes. It can be directly adapted and extended to flexible substrates such as the ones based on polyethylene terephthalate.[31] In addition to the periodical array of identical

microlenses, disordered configurations (in both the position and size distribution of the lenses) have been recently proposed. For example, such ensembles were obtained spontaneously using a phase separation technique,[32] or almost autonomously via the so-called "microbial approach."[33] Their integrated η_{ext} enhancement could not overcome that obtained with regular MLA, but adding disorder enabled improving the uniformity of the luminance angular distribution while suppressing spectral distortion. Lastly, in their recent work, Kim et al.[34] combined all the previously mentioned attributes (patterning on a flexible polyethylene naphthalate substrate, cost-effective fabrication process based on the self-assembly of microparticles, patterning of irregular MLA) and enhanced the MLA properties by incorporating Al_2O_3 nanoparticles. Due to the improved light extraction thanks to the nanoparticles scattering, the maximum power efficiency increased from 2.10 $lm.W^{-1}$ (irregular MLA) to 2.38 $lm.W^{-1}$ (irregular MLA including Al_2O_3 nanoparticles). In addition, the authors demonstrated that the nanoparticles block the penetration of oxygen and water vapor molecules into the organic layers, so that this approach also helps in improving the stability of the devices.

3 Improvement of the Internal Outcoupling

Unlike the MLA approach discussed in Sec. 2, micro- and nanostructures aimed at increasing the internal outcoupling are much more challenging to design since they are directly implemented within the thin film stack and as such can potentially degrade the electrical characteristics of the device. In the following, we report on different configurations which address those two aspects, namely improved internal outcoupling properties and an almost unaffected (or even ameliorated) electrical behavior. As will be discussed, they can be introduced in association with MLA to further enhance the light extraction of the OLED.

3.1 *Optimization of the Organic Light-Emitting Diodes Planar Stack*

As was exemplified in Fig. 3, the outcoupling efficiency strongly depends on the OLED layers' thicknesses in a planar architecture. The optical optimization of such a stack can be carried out by simulations, yet the proper modeling of the device requires a good knowledge of the optical indices employed (including their anisotropy[7]), as well as of the emitters' orientation and distribution profile. Alternatively, an empirical optimization can be undertaken by producing several samples with diverse thicknesses. However, this method is demanding in terms of time and materials consumption. Moreover, the batch-to-batch variability may complicate the analysis of the results, which calls for a simplified single-step approach. This can be easily realized using the horizontal dipping ("H-dipping") technique, regardless of the emitter type considered.[35] For the sake of demonstration, H-dipping was exploited to steadily increase the emissive layer thickness from 10 to 120 nm over a multiactive areas device.[36] This thickness gradient was directly obtained by continuously increasing the velocity of the coating bar during deposition. Using this one-pass process, a wedge-shaped device was fabricated, and the opto-electrical characteristics of the OLEDs were analyzed as a function of the active layer thickness. This methodology can be generalized to any layer, e.g., to the hole injection one (see Fig. 6). By varying its

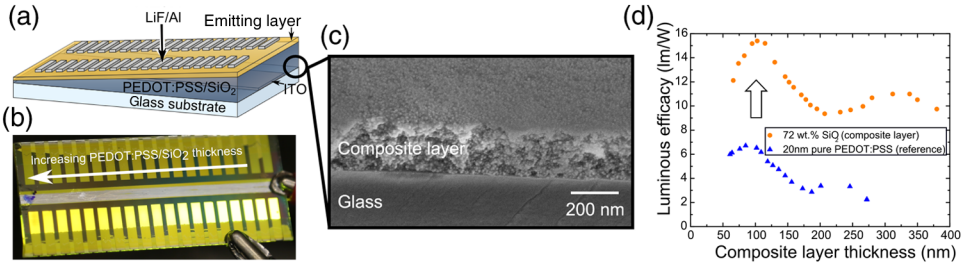

Fig. 6 (a) Schematic and (b) photograph of the device including the wedge-shaped composite layer, (c) SEM cross-section view of a PEDOT:PSS/SiO_2 composite layer and (d), influence of the hole injection layer thickness on the OLED luminous efficacy for both a pure PEDOT:PSS layer (reference) and a composite layer with 72 wt. % SiO_2.

corresponding thickness, the cavity effect can be optimized in a similar way. However, the device efficiency gain may be limited by an increased amount of parasitic absorption, eventually combined with a degradation of the charge transport. To go further, the H-dipping approach can be modified for the incorporation of advanced materials that feature low absorption and improved electrical properties and that can still be easily wet-processed. Such a material was recently fabricated by making a composite layer consisting of poly(3,4-ethylenedioxythiophene)-poly (styrenesulfonate) (PEDOT:PSS) and silica nanoparticles, as shown in Fig. 6(c).[37] Owing to the small nanoparticles' diameter (only around 7 nm), the modified hole injection layer possessed a haze factor below 1%, and the optical properties of the weak microcavity could be adjusted without introducing any scattering effects or parasitic absorption. The composite layer thickness was then varied between 50 and 400 nm. A luminous efficacy increase of up to 85% was measured for a layer thickness of 100 nm with respect to a 20-nm thick PEDOT:PSS-based reference device. This enhancement was related to a more favorable cavity configuration (improved coupling to the radiation modes), and on the electrical side, to a better hole vertical transport and injection following the inclusion of the nanoparticles network.

The latter aspect was also highlighted in a similar OLED stack but featuring SiO_2 (20 to 30 nm in diameter) and TiO_2 (20 to 130 nm in diameter) nanoparticles clustered between the emitting layer and the cathode.[38] In this configuration, an electroluminescence efficiency increase of up to 300% was measured by using a nanoparticle-free device as a reference. This was not attributed to an optical (scattering) effect. Instead, the enhancement was found to originate from an improved η_{int} due to the nanoparticles covering the cathode surface. Indeed, this partial coverage was believed to enhance the fields locally, leading to a better electron injection and, therefore, to an ameliorated charge balance. Thus, nanoparticles-based composite layers can be used as multifunctional elements that simultaneously act as an optical spacer for optimizing cavity effects and improve the interfacial properties of planar OLEDs.

3.2 *Micrometer Scale Corrugations for Waveguide Modes Outcoupling*

As discussed in Sec. 1, the anode and organic layers sandwiched between the substrate and the metallic cathode form a slab waveguide. Therefore, a significant part of the dissipated power is injected into the waveguide modes.

In order to limit this effect, a micron-scale optical perturbation of the anode can be exploited. Thus, micropatterned indium-tin oxide (ITO) anodes were realized by combining a photolithography and a wet etching step,[39] or alternatively, by sputtering an ITO layer through the gaps created by a self-assembly of microspheres,[40] prior to the deposition of PEDOT:PSS and of the remaining stack. To increase the refractive index contrast at the anode level, a low refractive index material can be inserted within the micromesh, as proposed in Ref. 41. In the WOLED investigated, a two-dimensional (2-D) square array of micro-columns was introduced within the ITO anode. The material chosen to form those micro-columns was MgF_2. In addition to its chemical stability, this material benefits from a low refractive index (around 1.38) compared with the ITO matrix (refractive index ranging from 1.8 to 2.1). As a result, it induces a modification of the modal distribution within the device. The fabrication route of this perturbed anode is shown in Fig. 7. The parameters (periodicity and columns diameter) were first defined in a resist layer by optical lithography, the 2-D array of micro-holes was then transferred into the ITO anode by wet etching, and this patterned matrix was filled by MgF_2 via a lift-off step. The duration of the MgF_2 vacuum deposition enabled to control the columns' height.

The micro-columns' height and interdistance were optimized empirically by measuring the efficiency enhancement in comparison to a similar but unperturbed WOLED as a reference. The materials and architecture of the devices were similar to the ones described in Sec. 2. Nine configurations with different spacing values (5, 10, and 15 μm) and column heights (33, 66, and 100 nm) but with a fixed diameter of 2.5 μm were studied. The results revealed a maximum efficiency enhancement of 38% obtained for a column distance and height of 5 μm and 66 nm, respectively. Increasing the spacing between the microcolumns reduced the perturbation introduced, therefore reducing its impact on the internal outcoupling. On the other hand, very small spacing values (well below 5 μm) should result in a strong decrease of the active area since MgF_2 is an insulator. The existence of an absolute optimum value can then be expected.

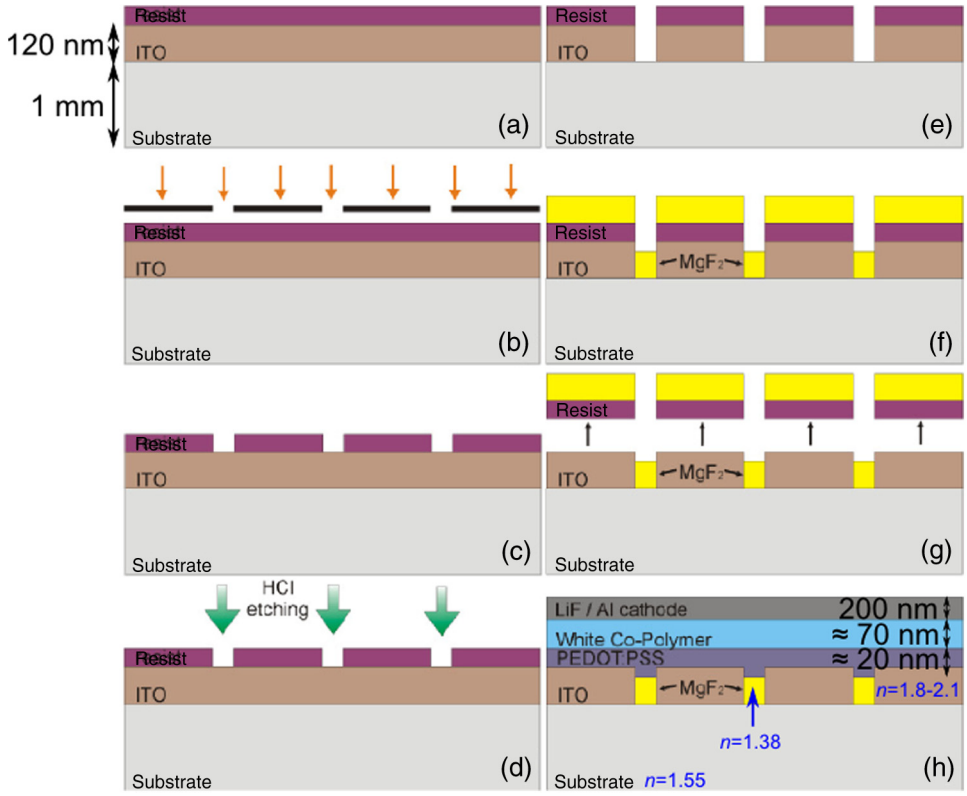

Fig. 7 Fabrication of the MgF_2 microcolumns for the extraction of waveguide modes (figure adapted from Ref. 41).

Similarly, the optimum height should result from a trade-off between a sufficient optical perturbation and good electrical characteristics of the WOLED. It was shown by simulation that in the absence of the microcolumns, a waveguide mode was mainly propagating within the ITO layer. On the contrary, in the perturbed configuration, no waveguide mode existed at the position of the low refractive index columns, and light was preferentially coupled to substrate or radiation modes. Interestingly, adding an MLA to the MgF_2-WOLED led to an efficiency increase of 50%, which is a similar enhancement factor as for the unperturbed WOLED with the MLA (see Fig. 5). Thus, it could be concluded that the microcolumns distributed equally the dissipated power of the waveguide modes into the substrate and radiation modes. By using this microphotonics approach, a luminous efficacy enhancement of 38% was obtained without modifying the emission and electrical characteristics of the device.

Unlike the previous example, microspherically textured OLEDs can enhance waveguide modes extraction while increasing the active area of the devices.[42] In this approach, an ITO-free OLED stack with PEDOT:PSS electrode was deposited on top of silica microspheres

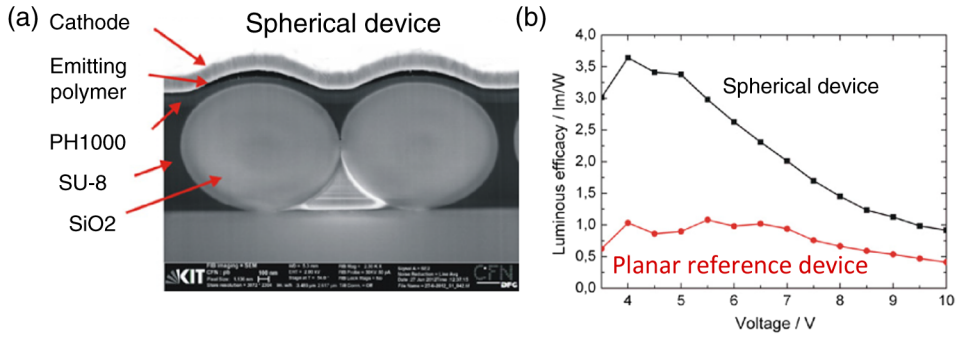

Fig. 8 (a) SEM cross-section view of the micro-spherically textured WOLEDs and (b) luminous efficacy of those devices with respect to equivalent but planar devices (adapted from Ref. 42).

with a diameter of 1.55 μm partially embedded into a 1.55 refractive index photoresist layer. This led to the curved waveguide configuration shown in Fig. 8(a).

In addition to the simplicity of the fabrication process, this method enabled to achieve a luminous efficacy enhancement of up to 3.7 [at 5 V, see Fig. 8(b)] compared with a planar equivalent WOLED, with otherwise unchanged emissive or electrical characteristics. In essence, three factors were evoked for explaining that improvement: a $\approx 4/3$ increase of the active area by comparison with a planar layout, a better extraction of the waveguide modes allowed by the waviness of the thin film stack, and eventually a more efficient outcoupling of the substrate modes. Indeed, the curved cathode can change the propagation angle of the reflected light, and thereby reduces TIR effects at the glass/air interface.

In Sec. 3.3, we will see that even higher enhancements can be achieved using adapted nanostructures in the vicinity of the active layer, although this may come along with a modification of the emission pattern which needs to be corrected.

3.3 *One-Dimensional High-Refractive Index Nanogratings for Efficient Waveguide Mode Extraction*

The advantage of nanostructures, such as one-dimensional (1-D) Bragg nanogratings, with respect to their micrometer-based counterpart is that stronger optical perturbations can be applied to waveguide modes. Periodic wavelength scale patterns were successfully tested in OLEDs in the early 2000s.[43–46] Still today, research efforts are ongoing to maximize the refractive index contrast using innovative solutions, e.g., by inserting high-n nanoparticles in a resist matrix that can be easily nanoimprinted,[47] and by fabricating periodically arranged air gaps giving rise to a refractive index difference as high as 0.9.[48] Regardless of the materials involved, two intrinsic limitations of this approach are the angular dependence of the resulting emission spectrum and the wavelength selectivity. Consequently, Bragg nanogratings appear to be more adapted to monochromatic devices than to WOLEDs. In the following examples, we will show that those nanostructures can interact not only with the waveguide modes but also with the substrate modes, and more generally with all the optical channels of the OLED, and demonstrate that they can be efficient and compatible with WOLEDs if combined with a proper external outcoupling method.

The first case discussed in this section is based on an ITO-free OLED incorporating a 1-D Bragg nanograting based on Ta_2O_5.[49] A cross-section view and the fabrication process of this device are shown in Fig. 9.

Ta_2O_5 was selected because it is a highly transparent material, and possesses a high-refractive index ($n = 2.1$ at 550 nm), which contrasts with that of the PEDOT:PSS anode ($n = 1.5$). The period was adjusted for the peak emission wavelength (550 nm) by using Bragg scattering such that the waveguide modes scatter with an angle lower than that of the escape cone.[2] To test the influence of the grating depth, the latter was varied between 48 and 77 nm. The angle resolved electroluminescence measurements of the yellow OLEDs underlined an emission

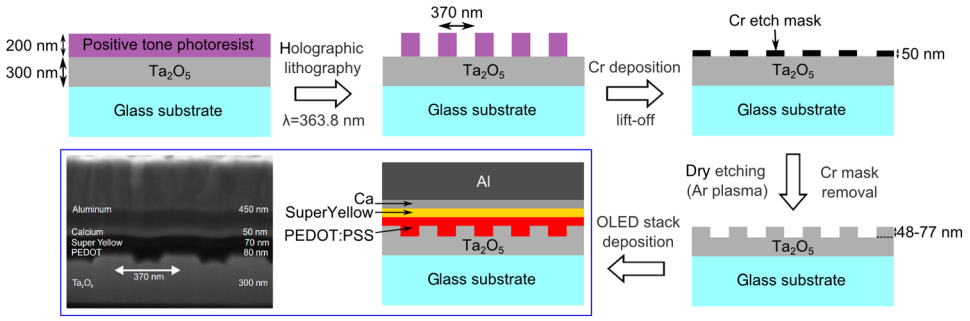

Fig. 9 Fabrication process of the Ta_2O_5 nanopatterned OLED based on a holographic lithography and a dry etching step. A SEM cross-section view of the final device is also reported (adapted from Ref. 49).

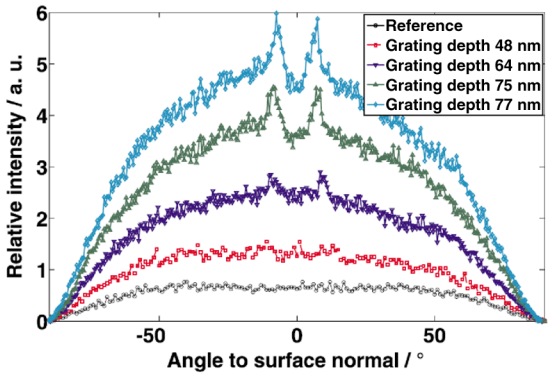

Fig. 10 Angle resolved emission obtained at 550 nm for the different grating depths investigated and compared to that of an unpatterned reference (figure from Ref. 49).

increasing with the grating depth (see Fig. 10). In particular, it could be shown that for the 77-nm deep grating, the emission was enhanced by up to 300% compared with an unpatterned OLED.[49] A remarkable feature of Fig. 10 is the presence of emission peaks at ± 8 deg for the three deepest gratings which result from the efficient outcoupling of the first-order transverse electric (TE_1) mode. Because the waveguide modes of different orders have less spatial overlap with the grating or a negligible filling factor in the active layer, they did not give rise to intense emission peaks. However, the extraction of the TE_1 mode observed at discrete angles was not sufficient to explain the overall emission increase observed. This was attributed to the outcoupling of substrate modes which account for a large part of the confined light in this particular layout. Indeed, the nanograting was also able to redirect the light trapped in the substrate modes.

Thus, it was possible to evidence experimentally the outcoupling of specific waveguide modes and highlight the capability of the grating to tackle simultaneously the internal and external outcoupling. Furthermore, the emitted light intensity was steadily enhanced by increasing the grating depth.

In the second example, we will see that this last property cannot be generalized, and that one needs to consider the complex interplay between the different optical channels in the design of efficient nanogratings. The structure considered for that purpose is based on a 1-D Bragg grating made of TiO_2 (n around 2.5 to 3.2 over the visible range) formed on top of the ITO anode of a WOLED using the materials and architecture as described in Sec. 2.[2] Its fabrication process, using a holographic lithography step, is shown in Fig. 11. As shown in this figure, a MLA was also added on the glass substrate for the two configurations investigated (grating height of 15 or 35 nm).

The efficiency enhancement factors measured after the introduction of the nano- and microstructures are shown in Fig. 12. The highest efficiency improvement was obtained for the 15-nm grating, due to an efficient outcoupling of the waveguide modes (mainly TE polarized), in combination with the MLA for the substrate modes extraction. Two additional conclusions arise from this figure. First, it can be observed that increasing the grating depth to 35 nm degrades the enhancement factor. Indeed, as was demonstrated experimentally by Hauss et al.,[4] the introduction of a Bragg grating impacts both the outcoupling from waveguide modes into radiation modes and the incoupling from radiation modes into waveguide modes. In Fig. 12, both configurations have a stronger outcoupling and thus lead to improved efficiencies. However, the 35-nm grating WOLED suffers from a higher incoupling into waveguide modes than for the 15-nm grating case. This effect limits the resulting enhancement factor. In other words, when incoupling mechanisms dominate over outcoupling ones, the introduction of a Bragg grating degrades the efficiency with respect to the unpatterned reference device.[4] The second comment is related to the different gains obtained after the introduction of the MLA. Those values tend to indicate that the in- and outcoupling of substrate modes into radiation and waveguide modes is also influenced by the geometry of the grating, and that the different optical channels are interdependent. Hence, the grating design is not trivial and should be carried out with optical simulations for optimized utilization conditions. Lastly, it should be pointed out that in all cases,

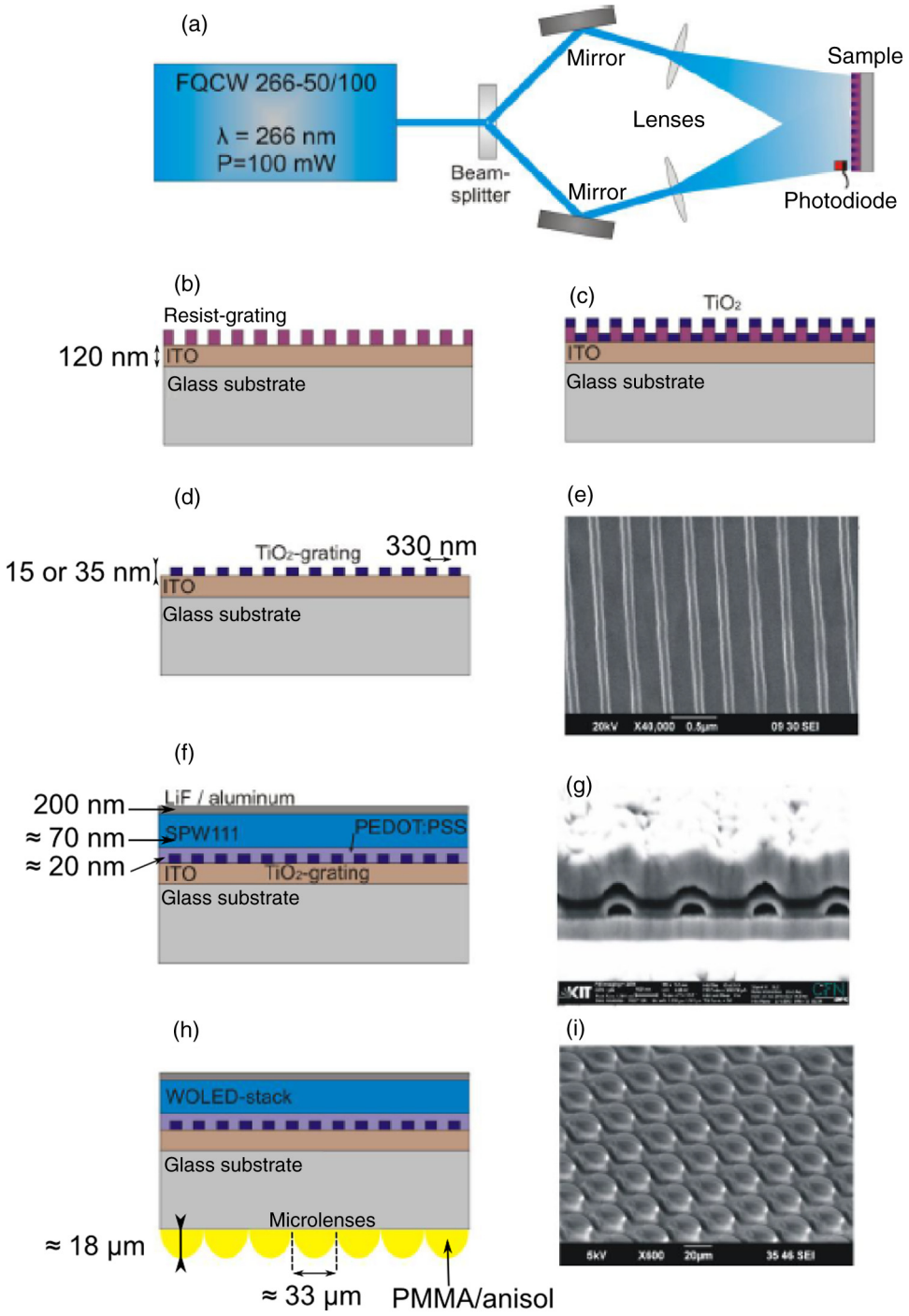

Fig. 11 (a)–(e) Fabrication of the TiO_2 Bragg grating via holographic lithography and vacuum deposition, (f)–(g) deposition of the WOLED stack and (h)–(i) addition of the MLA on the backside of the glass substrate. (g) The cross-section of the device shows a corrugation throughout the whole WOLED (figure adapted from Ref. 2).

the addition of the MLA enabled to suppress the grating features on the angular emission spectra, giving rise to a uniform white emission.

To conclude this section, the nanogratings introduced within the OLED stack can be exploited to simultaneously outcouple the waveguide and the substrate modes due to the interplay between the different optical channels. Even though Bragg gratings introduce angular dependencies on the emission spectra, this drawback can be overcome by using light diffusers such as a MLA.

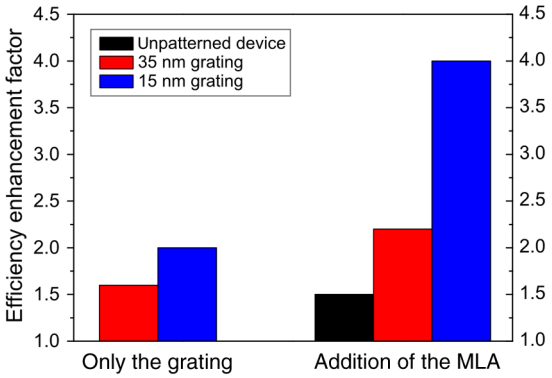

Fig. 12 Efficiency enhancement factors calculated by using an unpatterned WOLED without the MLA as a reference (adapted from Ref. 2).

3.4 *Internal Scattering Layers Based on Nanoparticles*

With a view to implementing outcoupling structures into an OLED manufacturing process, producing wet-processable and large area layers that do not require any lithography or vacuum-operated step is a major advantage [see the previous example in Fig. 8(a), or the scattering pixels in Fig. 13(a)]. In this context, scattering layers based on nanoparticles are industrially relevant candidates that can improve the outcoupling of substrate modes when deposited onto the substrate,[50] as well as internal modes (including waveguide and SPP modes provided that their spatial mode overlap with the scattering film is high enough[51]) if they are inserted within the OLED thin film stack.[52–55] In general, the nanoparticles' concentration should be tuned to avoid backward scattering. However, in the case of translucent/bidirectional OLEDs, this effect can be exploited on purpose to simultaneously improve light extraction in both the forward and backward directions, as demonstrated by Chang et al.[56] In Sec. 3.1, the concept of a hole injection layer (PEDOT:PSS) loaded with silica nanoparticles was introduced to modify the weak microcavity. Indeed, the densely packed nanoparticles embedded in the polymer layer formed an optically homogeneous layer (in the visible regime), whose thickness could be easily

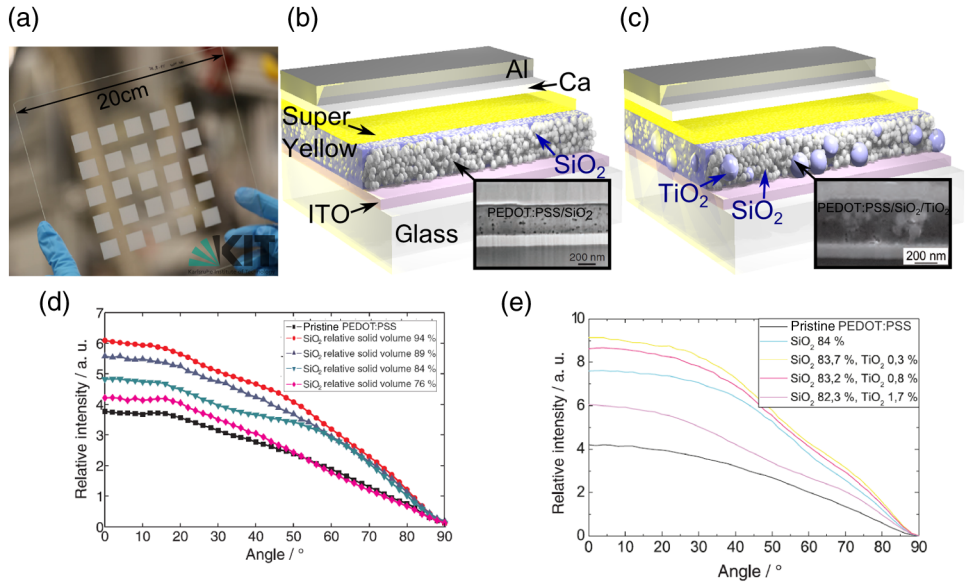

Fig. 13 (a) 5×5 array of scattering layers deposited in ambient conditions by screen printing over a 20×20 cm^2 glass substrate. Schematics of an OLED based either on (b) a scattering PEDOT:PSS/SiO_2 layer, or (c) a scattering layer made of PEDOT:PSS/SiO_2/TiO_2 (SEM cross-sections of the OLEDs shown in insets). The corresponding angularly resolved photoluminescence of those devices is reported in (d) and (e), respectively.

adjusted. The morphology of this low-absorbing composite layer can also be modified to introduce volume scattering by increasing the nanoparticles' diameters (e.g., to 20 or 30 nm,). By doing so, and after tuning the silica volume fraction, the device shown in Fig. 13(b) could be obtained.[57] With respect to an equivalent OLED without nanoparticle, its luminous efficiency increased by 66%, resulting from a better η_{int} (see end of Sec. 3.1 for explanations), and from an improved outcoupling [Fig. 13(d)]. Due to the low refractive index contrast between the nanoparticles and the polymer matrix, the scattering effect involved most presumably arose from bulk defects, namely air voids distributed throughout the composite layer. Air voids act as scattering centers, and as numerically shown in Ref. 58, their concentration should be optimized to ensure a good trade-off between the scattering properties and the resulting effective refractive index. A similar morphology was reported for silica nanoparticles based layers inserted between the hole injection and emissive layers. In that case, the corresponding devices exhibited a stronger scattering responsible for a noticeable change in the angular emission profile. To reinforce this scattering effect, TiO_2 nanoparticles (with a solid volume ratio below 2%, diameters ranging between 20 and 130 nm and a refractive index around 2.5 to 2.7) can be added inside the composite layer without significantly increasing its absorption coefficient [Fig. 13(c)].[59,60] For the best configuration investigated, the sole addition of TiO_2 nanoparticles led to a relative increase of 20% in both the electroluminescence and photoluminescence [Fig. 13(e)] measurements. This observation indicates that the luminous efficacy enhancement obtained in such a device mostly originates from optical effects, that is from a more efficient outcoupling of the modes by volume scattering.

3.5 *Optical Simulations of Internal Scattering Layers Based on Nanoparticles*

Numerical simulations of the light propagation in the device are an important tool in quest of an optimal outcoupling structure for a given OLED geometry. For that purpose, the emitting molecule can be modeled by means of a classical point dipole source.[3] However, the numerical schemes to simulate OLEDs with internal outcoupling are as manifold as the structures that have been suggested. The finite element method and the finite difference time domain (FDTD) method are frequently used due to their great flexibility.[61–65] However, the numerical effort grows fast with the considered volume and can rapidly exceed the capabilities of state of the art computers. Further modeling approaches include (but are not restricted to): mode-matching techniques,[66] coupled-mode approaches,[67,68] layered-medium Green's tensor methods[69,70] or ray optics.[71] Each approach has inherent advantages and disadvantages in terms of required computational time and hardware resources as well as of the accuracy of the resulting efficiency estimations.

As pointed out in Sec. 3.4, scattering layers based on nanoparticles are a particularly relevant class of internal outcoupling structures. Recent efforts in our group have therefore been dedicated to the development of a simulation tool that allows estimating the outcoupling efficiency of devices integrating such layers, out of wave optics calculations.[72] In contrast to previous numerical studies, coherent multiple scattering and near field effects (such as evanescent coupling to waveguide modes) are taken into account rigorously.

The underlying formalism makes use of the T-matrix formulation[73,74] of the scattering at the individual particles. The particle ensemble is modeled as a coupled system of N individual scatterers. The incident field at each particle contains the scattered fields from all other particles (in addition to the primary dipole excitation). Both the direct interaction as well as the reflections from the layer interfaces need to be accounted for (see Fig. 14). Therefore, the electromagnetic fields are transformed from the spherical wave representation to a superposition of plane waves.[75,76] Their propagation can then be treated analytically by means of the transfer matrix or the scattering matrix algorithm.[72] With an efficient scheme for the numerical evaluation of the so-called Sommerfeld integrals that occur in the analysis, the interaction of a large number of particles can be accurately simulated.[77] However, the number of particles still needs to be truncated to limit the necessary simulation time. As a consequence, the outcoupling efficiency is systematically underestimated in the simulations. An elegant way to estimate and correct for this error was proposed in Ref. 78. By repeating the simulation for an increasing width of the scattering structure, the outcoupling efficiency as a function of the lateral dimension of

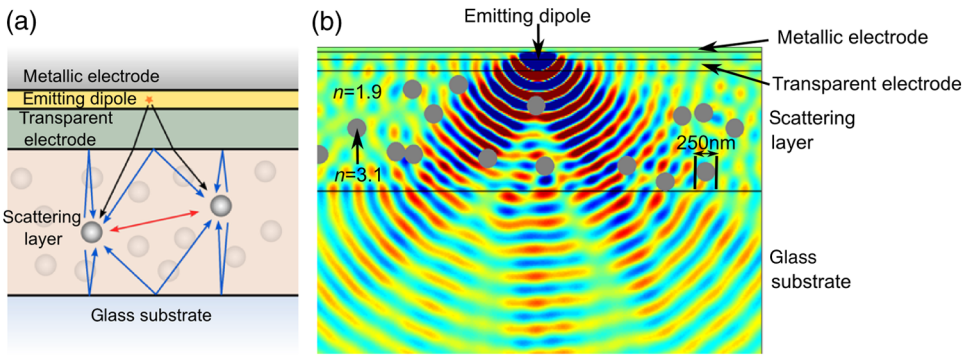

Fig. 14 (a) Schematic view of the coupling between two nanoparticles. The arrows represent the initial dipole excitation (in black), the direct interaction, i.e., the scattered field of one particle that is then incident to the other (in red), as well as the layer system's reflections of the scattered field that is then incident to the other particle (in blue). (b) Detail of the simulated three-dimensional electric field distribution for a typical OLED structure with a 1.6-μm thick scattering layer including spherical nanoparticles.

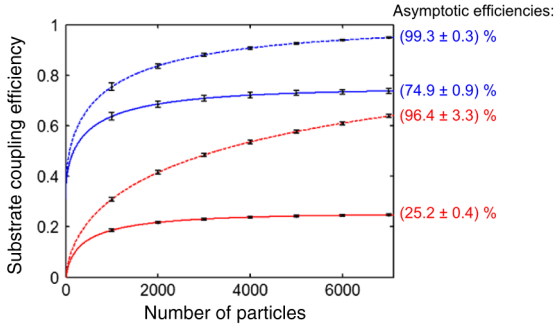

Fig. 15 Substrate coupling efficiency plotted as a function of the particles' number at fixed volume concentration for a typical OLED geometry with scattering particles. The blue and red lines correspond to parallel and perpendicular dipole moment orientation, and the solid and dashed lines correspond to the realistic structure and to a structure without absorption losses, respectively.

the scattering layer can be fitted by a phenomenological expression that then allows for an extrapolation to infinite scattering samples.

As an application example, we show in Fig. 15 simulation results for a realistic layer stack including a TiO_2 nanoparticles-based scattering layer. The layer system parameters were chosen to reproduce the OLED stack named "device H" in the study of Chang et al.[79] In addition, an ideal layer stack of lossless materials was considered to demonstrate the validity of the approach by checking the conservation of energy. All calculations were run at a vacuum wavelength of 520 nm. Figure 15 shows the simulated substrate coupling efficiency, i.e., the power radiated into the substrate layer divided by the total dissipated power, as a function of the number of scattering particles at a fixed particle volume concentration of 3.25 %. Without absorption, all waveguided power is expected to eventually be outcoupled if the lateral extent of the scattering layer tends to infinity. In fact, an asymptotic efficiency around 100% was extrapolated for the ideal device, indicating the validity of the simulations and of the extrapolation scheme. For the realistic device parameters, the outcoupling from the thin film waveguide modes competes with the mode decay due to absorption, resulting in an efficiency well below 100%. In the given example, the substrate coupling efficiency converges to ≈75% (≈25%) in the case of a parallel (perpendicular) dipole moment orientation relative to the layer interfaces. This is a significant enhancement compared with the theoretical substrate coupling efficiency of 68% (3%) for the case without scattering particles.

We conclude that a prediction of the outcoupling efficiency for OLEDs with internal scattering particle layers based on rigorous wave optics calculations is feasible, paving the way for

computer assisted device optimization of OLEDs with an internal scattering particle layer. In fact, the scattering layer and the OLED stack cannot be regarded independently. An OLED layer system that has been optimized with regard to outcoupling efficiency without scattering layer is not necessarily optimal in combination with internal outcoupling structures. Although involving a non-negligible numerical effort, the method presented herein is much more time and cost effective than empirical and experimental surveys. In the future, it will allow for a simultaneous optimization of the scattering layer parameters and of the OLED stack.

4 Conclusion and Outlook

In this review, several photonic microstructures designed to extract the waveguide modes propagating within a solution-processed bottom-emitting WOLED stack have been introduced. Owing to the waviness of the thin film stack, microspherically textured devices were found to efficiently outcouple internal modes and could simultaneously improve substrate modes extraction while enhancing the active area on a given footprint. Alternatively, it was shown that Bragg gratings, if used in the right configuration, could be used in monochromatic devices to foster the coupling of internal modes to substrate and radiation modes. This approach could be successfully extended to WOLED by combining it with microlens arrays produced in an easy and versatile way. Indeed, the latter enabled to avoid the angular dependencies normally observed on the emission spectra, with a weak influence of the microlenses' diameter on the extraction efficiency. To facilitate the implementation of outcoupling structures in a manufacturing process flow, wet-processable layers were also presented, and the case of nanoparticles-loaded hole injection layers was exemplified. Depending on the size and material of the nanoparticles, scattering effects could be avoided to solely optimize cavity effects, or conversely, intentionally strengthened to extract both internal and substrate modes by volume scattering. We demonstrated that the optimization of the scattering layer parameters can be performed numerically by exploiting an algorithm based on the T-matrix formalism for the scattering by individual particles, and on the scattering matrix algorithm for the propagation through a system made of planar interfaces. Interestingly, the composite layers reported here improved both the optical and electrical properties of the devices, notably by a modification of the charge injection and vertical transport. Lastly, it is worth noting that a prospective concept was recently investigated by numerical means to achieve single-pass light extraction from the OLED front layer (glass substrate for bottom-emitting OLEDs or cathode/anode in the case of top emitting/inverted top emitting devices) while preserving the original angular distribution profile.[80] It was realized using transformation optics to design a graded refractive index structure between the exit facet and the free space and as such, could be used for waveguide or substrate modes extraction. This approach, primarily developed for pixelated and monochromatic devices, showed promising outcoupling properties for experimentally accessible refractive indices, and opens new perspectives for photon management in OLEDs.

Acknowledgments

G.G. acknowledges the support of the Helmholtz Postdoctoral Program. J.B.P. and A.E. gratefully acknowledge financial support from the Karlsruhe School of Optics & Photonics (KSOP). This work was partly carried out with the support of the Deutsche Forschungsgemeinschaft (DFG) through program DFG-SPP 1839 "Tailored Disorder."

References

1. C. Adachi et al., "Nearly 100% internal phosphorescence efficiency in an organic light-emitting device," *J. Appl. Phys.* **90**, 5048–5051 (2001).
2. T. Bocksrocker et al., "White organic light emitting diodes with enhanced internal and external outcoupling for ultra-efficient light extraction and Lambertian emission," *Opt. Express* **20**(106), A932–A940 (2012).

3. R. R. Chance et al., "Molecular fluorescence and energy transfer near interfaces," *Adv. Chem. Phys.* **37**(1), 65 (1978).
4. J. Hauss et al., "On the interplay of waveguide modes and leaky modes in corrugated OLEDs," *Opt. Express* **19**(104), A851–A858 (2011).
5. R. Meerheim et al., "Quantification of energy loss mechanisms in organic light-emitting diodes," *Appl. Phys. Lett.* **97**(25), 253305 (2010).
6. E. M. Purcell, "Spontaneous emission probabilities at radio frequencies," *Phys. Rev.* **69**, 681 (1946).
7. M. Flämmich et al., "Orientation of emissive dipoles in OLEDs: quantitative in situ analysis," *Org. Electron.* **11**(6), 1039–1046 (2010).
8. M. J. Jurow et al., "Understanding and predicting the orientation of heteroleptic phosphors in organic light-emitting materials," *Nat. Mater.* **15**, 85–91 (2016).
9. T. D. Schmidt et al., "Efficiency analysis of organic light-emitting diodes based on optical simulations," *IEEE J. Sel. Top. Quantum Electron.* **19**(5), 1–12 (2013).
10. J. A. E. Wasey et al., "Efficiency of radiative emission from thin films of a light-emitting conjugated polymer," *Phys. Rev. B* **64**(20), 205201 (2001).
11. A. G. Fluxim, "SETFOS: Semiconducting emissive thin film optics simulator software," http://www.fluxim.com
12. J. S. Kim et al., "Electroluminescence emission pattern of organic light-emitting diodes: Implications for device efficiency calculations," *J. Appl. Phys.* **88**(2), 1073–1081 (2000).
13. D. S. Mehta et al., "Light out-coupling strategies in organic light emitting devices," in *Proc. ASID*, **6**(2), 198–201 (2006).
14. K. Saxena et al., "A review on the light extraction techniques in organic electroluminescent devices," *Opt. Mater.* **32**(1), 221–233 (2009).
15. M. Furno et al., "Outcoupling efficiency in small-molecule OLEDs: from theory to experiment," *Proc. SPIE* **7617**, 761716 (2010).
16. A. I. Zhmakin, "Enhancement of light extraction from light emitting diodes," *Phys. Rep.* **498**(4), 189–241 (2011).
17. K. Hong et al., "Review paper: Recent developments in light extraction technologies of organic light emitting diodes," *Electron. Mater. Lett.* **7**(2), 77–91 (2011).
18. W. Brütting et al., "Device efficiency of organic light-emitting diodes: Progress by improved light outcoupling," *Phys. Status Solidi A* **210**(1), 44–65 (2013).
19. M. C. Gather et al., "Recent advances in light outcoupling from white organic light-emitting diodes," *J. Photonics Energy* **5**(1), 057607 (2015).
20. S. Ho et al., "Review of recent progress in multilayer solution-processed organic light-emitting diodes," *J. Photonics Energy* **5**(1), 057611 (2015).
21. A. R. Duggal et al., "Solution-processed organic light-emitting diodes for lighting," *J. Display Technol.* **3**(2), 184–192 (2007).
22. T.-W. Koh et al., "Enhanced outcoupling in organic light-emitting diodes via a high-index contrast scattering layer," *ACS Photonics* **2**(9), 1366–1372 (2015).
23. W. Wu et al., "Nanocellulose-based translucent diffuser for optoelectronic device applications with dramatic improvement of light coupling," *ACS Appl. Mater. Interfaces* **7**(48), 26860–26864 (2015).
24. Y. Yao et al., "Light management in plastic-paper hybrid substrate towards high-performance optoelectronics," *Energy Environ. Sci.* **9**, 2278 (2016).
25. C. F. Madigan et al., "Improvement of output coupling efficiency of organic light-emitting diodes by backside substrate modification," *Appl. Phys. Lett.* **76**(13), 1650–1652 (2000).
26. S. Möller et al., "Improved light out-coupling in organic light emitting diodes employing ordered microlens arrays," *J. Appl. Phys.* **91**(5), 3324–3327 (2002).
27. M. K. Wei et al., "Method to evaluate the enhancement of luminance efficiency in planar OLED light emitting devices for microlens array," *Opt. Express* **12**(23), 5777–5782 (2004).
28. M. K. Wei et al., "The influence of a microlens array on planar organic light-emitting devices," *J. Micromech. Microeng.* **16**(2), 368 (2006).
29. T. Bocksrocker, "Technologien für das Lichtmanagement in organischen Leuchtdioden," PhD Thesis, Karlsruher Institut für Technologie (2013).

30. F. Mayer et al., "Cloaking contacts on large-area organic light-emitting diodes," *Adv. Opt. Mater.* **4**, 740–745 (2016).
31. A. Egel et al., "Extracting substrate modes from flexible OLEDs," in *Solid-State and Organic Lighting, DT2E-3* (2013).
32. K. Lee et al., "Simultaneously enhanced device efficiency, stabilized chromaticity of organic light emitting diodes with lambertian emission characteristic by random convex lenses," *Nanotechnology* **27**(7), 075202 (2016).
33. S. Mehta et al., "Microbes based printing for fabrication of microlenses for organic light emitting diodes," *Org. Electron.* **35**, 199–207 (2016).
34. Y. Y. Kim et al., "Novel microlens arrays with embedded Al_2O_3 nanoparticles for enhancing efficiency and stability of flexible polymer light-emitting diodes," *RSC Adv.* **6**, 65450 (2016).
35. B. Park et al., "Organic light-emitting devices fabricated using a premetered coating process," *Opt. Express* **17**(24), 21362–21369 (2009).
36. S. Höfle et al., "Influence of the emission layer thickness on the optoelectronic properties of solution processed organic light-emitting diodes," *ACS Photonics* **1**(10), 968–973 (2014).
37. J. B. Preinfalk et al., "Tuning the microcavity of organic light emitting diodes by solution processable polymer: nanoparticle composite layers," *ACS Appl. Mater. Interfaces* **8**(4), 2666–2672 (2016).
38. B. Riedel et al., "Polymer light emitting diodes containing nanoparticle clusters for improved efficiency," *Org. Electron.* **11**(7), 1172–1175 (2010).
39. T. W. Koh et al., "Optical outcoupling enhancement in organic light-emitting diodes: highly conductive polymer as a low-index layer on microstructured ITO electrodes," *Adv. Mater.* **22**(16), 1849–1853 (2010).
40. C. Y. Chen et al., "Analyses of optical out-coupling of organic light-emitting devices having micromesh indium tin oxide and conducting polymer as composite transparent electrode," *Opt. Express* **24**(10), A810–A822 (2016).
41. T. Bocksrocker et al., "Efficient waveguide mode extraction in white organic light emitting diodes using ITO-anodes with integrated MgF_2-columns," *Opt. Express* **20**(6), 6170–6174 (2012).
42. T. Bocksrocker et al., "Micro-spherically textured organic light emitting diodes: a simple way towards highly increased light extraction," *Org. Electron.* **14**(1), 396–401 (2013).
43. J. M. Lupton et al., "Bragg scattering from periodically microstructured light emitting diodes," *Appl. Phys. Lett.* **77**(21), 3340–3342 (2000).
44. B. J. Matterson et al., "Increased efficiency and controlled light output from a microstructured light-emitting diode," *Adv. Mater.* **13**(2), 123–127 (2001).
45. Y. R. Do et al., "Enhanced light extraction from organic light-emitting diodes with 2D SiO_2/SiN_x photonic crystals," *Adv. Mater.* **15**(14), 1214–1218 (2003).
46. M. Fujita et al., "Organic light-emitting diode with ITO/organic photonic crystal," *Electron. Lett.* **39**(24), 1 (2003).
47. A. Pradana et al., "Tailoring the refractive index of nanoimprint resist by blending with TiO_2 nanoparticles," *Opt. Mater. Express* **4**(2), 329–337 (2014).
48. Y. S. Shim et al., "An extremely low-index photonic crystal layer for enhanced light extraction from organic light-emitting diodes," *Nanoscale* **8**(7), 4113–4120 (2016).
49. B. Riedel et al., "Enhancing outcoupling efficiency of indium-tin-oxide-free organic light-emitting diodes via nanostructured high index layers," *Appl. Phys. Lett.* **96**(24), 243302 (2010).
50. C. H. Shin et al., "Nanoparticle scattering layer for improving light extraction efficiency of organic light emitting diodes," *Opt. Express* **23**(3), A133–A139 (2015).
51. H. W. Chang et al., "Nano-particle based scattering layers for optical efficiency enhancement of organic light-emitting diodes and organic solar cells," *J. Appl. Phys.* **113**(20), 204502 (2013).
52. D. Riedel et al., "Polymer-based scattering layers for internal light extraction from organic light emitting diodes," *Org. Electron.* **32**, 27–33 (2016).
53. H. W. Chang et al., "Organic light-emitting devices integrated with internal scattering layers for enhancing optical out-coupling," *J. Soc. Inf. Display* **19**(2), 196–204 (2011).

54. K. H. Kim et al., "Enhancing light-extraction efficiency of OLEDs with high-and low-refractive-index organic-inorganic hybrid materials," *Org. Electron.* **36**, 103–112 (2016).
55. C. H. Chang et al., "Improving the outcoupling efficiency of white organic light-emitting devices based on a gradient refractive index substrate," *Jpn. J. Appl. Phys.* **55**(3S1), 03CD01 (2016).
56. H. W. Chang et al., "Bi-directional organic light-emitting diodes with nanoparticle-enhanced light outcoupling," *Laser Photonics Rev.* **7**(6), 1079–1087 (2013).
57. B. Riedel et al., "Tailored highly transparent composite hole-injection layer consisting of pedot: PSS and SiO_2 nanoparticles for efficient polymer light-emitting diodes," *Adv. Mater.* **23**(6), 740–745 (2011).
58. J. Lee et al., "Enhancement of light-extraction efficiency of organic light-emitting diodes using silica nanoparticles embedded in TiO_2 matrices," *Opt. Express* **22**(103), A705–A714 (2014).
59. B. Riedel, "Effizienzsteigerung in organischen Leuchtdioden," PhD Thesis, Karlsruher Institut für Technologie (2011).
60. B. Riedel et al., "Polymer light-emitting diodes with inorganic nanocomposite interlayers for efficiency enhancement," *J. Photonics Energy* **1**(1), 011018 (2011).
61. L. Zschiedrich et al., "Numerical analysis of nanostructures for enhanced light extraction from OLEDs," *Proc. SPIE* **8641**, 86410B (2013).
62. Y. J. Lee et al., "A high-extraction-efficiency nanopatterned organic light-emitting diode," *Appl. Phys. Lett.* **82**(21), 3779–3781 (2003).
63. A. Chutinan et al., "Theoretical analysis on light-extraction efficiency of organic light-emitting diodes using FDTD and mode-expansion methods," *Org. Electron.* **6**(1), 3–9 (2005).
64. Y. J. Lee et al., "Far-field radiation of photonic crystal organic light-emitting diode," *Opt. Express* **13**(15), 5864–5870 (2005).
65. M.-C. Oh et al., "Hollow-core polymeric nanoparticles for the enhancement of OLED outcoupling efficiency," *Displays* **37**, 72–78 (2015).
66. P. Vandersteegen, "Modeling of the optical behavior of organic LEDs for illumination," PhD Thesis, Ghent University (2008).
67. R. F. Oulton et al., "Efficiency enhancement of organic based light emitting diodes using a scattering layer," arXiv preprint physics/0411095 (2004).
68. T. Schwab et al., "Coherent mode coupling in highly efficient top-emitting OLEDs on periodically corrugated substrates," *Opt. Express* **22**(7), 7524–7537 (2014).
69. H. Greiner et al., "Numerical modeling of light emission and propagation in organic LEDs using the Green's tensor," *Proc. SPIE* **5214**, 248–259 (2004).
70. Ö. Sepsi et al., "Polarized light emitting diodes using silver nanoellipsoids," *Opt. Express* **22**(104), A1190–A1196 (2014).
71. S. Altazin et al., "38.3: simulations, measurements, and optimization of OLEDs with scattering layer," *SID Symp. Digest Tech. Pap.* **46**(1), 564–567 (2015).
72. A. Egel et al., "Dipole emission in stratified media with multiple spherical scatterers: Enhanced outcoupling from OLEDs," *J. Quant. Spectrosc. Radiat. Transfer* **148**, 165–176 (2014).
73. P. C. Waterman, "Matrix formulation of electromagnetic scattering," *Proc. IEEE* **53**(8), 805–812 (1965).
74. M. I. Mishchenko et al., "T-matrix theory of electromagnetic scattering by particles and its applications: a comprehensive reference database," *J. Quant. Spectrosc. Radiat. Transfer* **88**(1–3), 357–406 (2004).
75. G. Kristensson, "Electromagnetic scattering from buried inhomogeneities—a general three-dimensional formalism," *J. Appl. Phys.* **51**(7), 3486–3500 (1980).
76. D. W. Mackowski, "Exact solution for the scattering and absorption properties of sphere clusters on a plane surface," *J. Quant. Spectrosc. Radiat. Transfer* **109**(5), 770–788 (2008).
77. A. Egel et al., "Efficient evaluation of Sommerfeld integrals for the optical simulation of many scattering particles in planarly layered media," *J. Opt. Soc. Am. A Opt. Image Sci. Vis.* **33**(4), 698–706 (2016).

78. C. Wiesmann, "Nano-structured LEDs–Light extraction mechanisms and applications," PhD Thesis, Universität Regensburg (2010).
79. C. H. Chang et al., "Fourfold power efficiency improvement in organic light-emitting devices using an embedded nanocomposite scattering layer," *Org. Electron.* **13**(6), 1073–1080 (2012).
80. M. F. Schumann et al., "Single-pass and omniangle light extraction from light-emitting diodes using transformation optics," *Opt. Lett.* **40**(23), 5626–5629 (2015).

Guillaume Gomard obtained his PhD in 2012 at the Lyon Institute of Nanotechnology (France) after investigating the potential of photonic crystals (PhCs) for improving the absorption in thin-film solar cells. Since 2013, he has been the group leader for the "Nanophotonics" activities at the Light Technology Institute (KIT, Germany). His current research encompasses the analysis of disordered PhCs, scattering stochastic ensembles, or hierarchical bioinspired photonic structures and their implementation within optoelectronic devices for enhanced efficiencies.

Jan B. Preinfalk received his Master of Science degree in electrical engineering at the Karlsruhe Institute of Technology (KIT), Germany, in 2013. Since 2014, he has been pursuing his PhD at the Light Technology Institute of the KIT on the topic of solution-processable technologies for light management in organic light-emitting diodes.

Amos Egel received his "Diplom-Physiker" degree from the Heidelberg University, Heidelberg, Germany in 2011. Currently, he is working toward his PhD in the department of electrical engineering at the Karlsruhe Institute of Technology (KIT), Karlsruhe, Germany. His research focuses on the optical modelling of nanostructures for light management in optoelectronic devices.

Uli Lemmer received his diploma degree from the RWTH Aachen University, Germany, in 1990 and his PhD from the University of Marburg, Germany, in 1995. From 1995 to 1996, he held a postdoctoral position with the University of California at Santa Barbara. He was with the University of Munich, Germany, from 1996 to 2002. In 2002, he was appointed as a full professor and director of the Light Technology Institute at KIT.